Low Temperature Fabrication of BiFeO3 Films on Aluminum Foils under an N2-Rich Atmosphere

Jing Yan *

Posted Date: 12 August 2024

doi: 10.20944/preprints202408.0798.v1

Keywords: BiFeO3; Aluminum foil; N2-rich atmosphere; Electric properties

 doi:10.20944/preprints202408.0798.v1

Article

Low Temperature Fabrication of $BiFeO_3$ Films on Aluminum Foils under an N_2-Rich Atmosphere

Jing Yan

College of Physics and Electronic Engineering, Qilu Normal University, Jinan, Shandong 250200, China; jndxclyj@163.com

Abstract: To be CMOS-compatible, a low preparation temperature (< 500 °C) of ferroelectric films is required. In this study, $BiFeO_3$ films were successfully fabricated at a low annealing temperature (< 450 °C) on aluminum foils by a metal-organic decomposition process. The annealing atmosphere on performance of $BiFeO_3$ films was assessed at 440 ± 5℃. By using an N_2-rich atmosphere, a large remnant polarization (P_r~78.1 μC/cm² @ 1165.2 kV/cm), a high rectangularity (~91.3% @ 1165.2 kV/cm) of the *P-E* loop, excellent charge-retaining ability up to 1.0×10^3 s and outstanding fatigue resistance after 1.0×10^9 switching cycles can be observed. By adopting an N_2-rich atmosphere and the aluminum foil substrates, decent electrical properties (P_r~70 μC/cm² @ 1118.1 kV/cm) of the $BiFeO_3$ films were achieved at a very low annealing temperature of 365 ±5 °C. These results offer a new idea for lowering the annealing temperature for integrated ferroelectrics in high-density FeRAM applications.

Keywords: $BiFeO_3$; aluminum foil; N_2-rich atmosphere; electric properties

1. Introduction

$BiFeO_3$ (BFO) has been extensively investigated as a promising multiferroic material in recent years [1–8]. Studies have reported on enhancing the ferroelectric properties of BFO films, such as introducing buffer layers, doping the isovalent or aliovalent ions, and domain engineering [9–17]. However, obtaining *P-E* hysteresis loops with high rectangularity in polycrystalline BFO films using chemical solution deposition methods remains a challenge, especially under low annealing temperature (< 500 °C). Most efforts have focused on improving the quality of BFO films [9–19], however, few studies have focused on the bottom electrode as well as the interface between the bottom electrode and film, though these factors remain equally important. In general, obtaining desired contact at the interface between the traditional substrate (such as Si) and film may be hardly achieved due to slight thermal deformation during low temperature (<500 °C) annealing treatment. Recently, Kingon *et al*. successfully obtained high quality $Pb(Zr_{0.52}Ti_{0.48})O_3$ films directly on base metal copper foils, providing a new strategy for choosing base metal foils as the bottom electrodes [20]. As a common base metal, aluminum (Al) foil may serve as an alternative electrode for BFO ferroelectric films, as Al_2O_3 can readily form a very dense, stable, and extremely thin (~5 nm) layer. This may effectively reduce the leakage current and lower the risk of breakdown. Furthermore, the thermal expansion coefficient of Al (23.8×10^{-6} /°C) [21] is much higher than that of Si (3.6×10^{-6}/°C) [22], thus the tight contact interface between the BFO film and Al substrate can be expected even at a low annealing temperature. In this work, aluminum foils were adopted as substrates for preparation of BFO films using the metal organic decomposition (MOD) method. High temperatures often cause serious problems, including interdiffusion, charged defects, phase decomposition, and valence fluctuations, and these issues can damage a film's electrical properties and performance stability [23]. To enhance the performance of BFO films and provide complementary metal oxide semiconductor (CMOS)-compatibility, a low processing temperature below 500 °C was required. The annealing atmospheres on properties of BFO films on Al substrates were discussed, it was found that an N_2-

 doi:10.20944/preprints202408.0798.v1

rich atmosphere can facilitate the crystallization of BFO films and thus lower the annealing temperature. Therefore, low temperature preparation for BFO films were attempted. By adopting an N_2-rich atmosphere and the aluminum foil substrates, decent ferroelectric properties (P_r~70 μC/cm²@ 1118.1 kV/cm) were obtained at a very low annealing temperature of 365 ±5 °C.

2. Materials and Methods

BFO films (~800 nm) were fabricated on mirror aluminum foils (Surface roughness~0.02±0.005 μm, thickness~0.3 mm. Size~10mm×10mm) using the MOD process. The precursor solution was prepared by dissolving bismuth nitrate and iron nitrate in acetic acid and ethylene glycol according to the stoichiometric ratio. 5 mol% excess bismuth was used to compensate the volatilization of Bi_2O_3. The ratio of acetic acid and ethylene glycol was 3:1, and the solution concentration was 0.1mol/L. The films were deposited onto the Al foils by spin coating and then annealed layer by layer for 10 min at 365~440±5°C in N_2-rich (BFO_N) or O_2-rich (BFO_O) atmospheres (During the annealing process, N_2 or O_2 is introduced at a rate of 1.5sccm.) Each layer of film was deposited onto the substrate by spin coating at 4000 rpm for 30 s. Au top electrodes were deposited using a sputtering system through a shadow mask with a diameter of 0.2 mm on the films. Crystallographic characteristics of BFO films were analyzed by using standard X-ray diffraction (XRD) 2θ-scans in a Dmax-2500PC diffractometer (Rigaku, Japan) equipped with a Ni-filtered Cu-Kα radiation source (λ = 1.54184 Å). Surface morphologies were characterized using a SU-70 thermal field emission scanning electron microscope (SEM) (Hitachi, Japan). The chemical bonding states of the constituent elements were analyzed using a Thermo Scientific™ K-Alpha™ (hν = 1486.6 eV) X-ray Photoelectron Spectrometer (Thermo Fisher Scientific, USA). The energy resolution and the spatial resolution of the spectrometer were 0.5 eV and 50 μm, respectively. A Precision Premium II ferroelectric tester (maximum voltage of 99.9 V, Radiant Technology, USA) was adopted to measure the ferroelectric properties and leakage currents. The soaking time was 500ms during leakage test under the unswitched linear mode.

3. Results and Discussion

3.1. Performance of $BiFeO_3$ under Different Atmospheres Annealed at 440 ± 5 °C

3.1.1. Microstructure Analysis

The polycrystalline perovskite structures with a bulk-like rhombohedral phase were obtained in both the BFO_N and BFO_O films at 440 ± 5°C [23], as shown in Figure 1. No secondary phase was observed. This demonstrated that the Al foil was a suitable substrate material for the preparation of BFO films. The global average grain size calculated via Scherrer formula for BFO_N and BFO_O films were shown in table1. The grain size of BFO_N film was larger than that of BFO_O film. Furthermore, the local average grain sizes via SEM analysis (Figure 2, from a statistical analysis of 100 grains via the Nano Measurer software) have also been shown in Table 1. The similar results can be indicated that the reduced atmosphere could facilitate grain growth. The difference between the global average grain size and the local one may be related to the grain size nonuniformity.

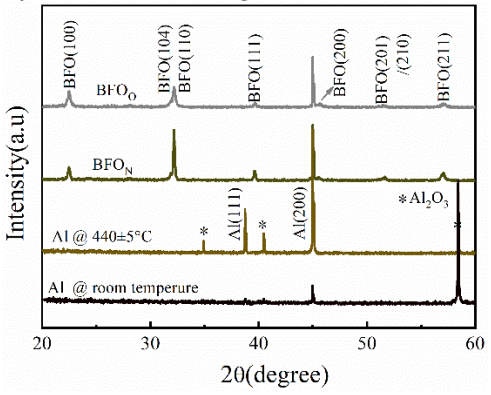

Figure 1. (Color online) X-ray diffraction (XRD) 2θ-scan patterns of the Al foil, BFO film deposited in N_2-rich and O_2-rich atmospheres at 440±5°C.

 doi:10.20944/preprints202408.0798.v1

Table 1. The average grain size for BFO_N and BFO_O films.

film		BFO_N	BFO_O
the global average grain size via Scherrer formula	(100) -oriented grains	180 nm	120 nm
	(111) -oriented grains	75 nm	50 nm
	(211) -oriented grains	30 nm	23 nm
the local average grain size via SEM analysis (using 100 grains)		105 nm	55 nm

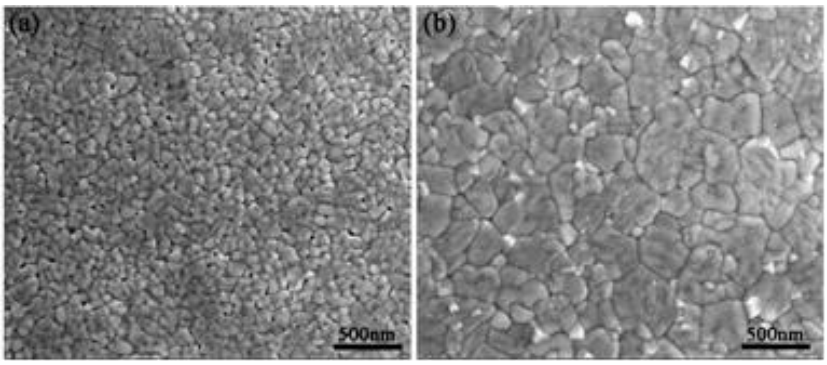

Figure 2. Surface SEM images for **(a)** the BFO_O and **(b)** BFO_N films at 440 ± 5°C.

Figure 2 shows the surface morphologies of the BFO films. A compact surface and larger grains were observed in the BFO_N films compared to the BFO_O films at 440 ± 5°C, possibly due to the higher content of oxygen vacancies under a reducing atmosphere than that of O_2 rich atmosphere. Reports have demonstrated that oxygen vacancies can facilitate the diffusion of ions during the annealing process [24]. As shown in Figure 2(b), the BFO_N film was mainly composed of large block-like grains, which could be ascribed to the presence of the grain merger phenomenon during the grain growth process. Notably, the observed white fine grains in surface of the BFO_N film may be Bi_2O_3 grains, because the relatively high content of oxygen vacancies in the BFO_N film possibly accelerated the diffusion of Bi_2O_3. As a result, significantly more Bi_2O_3 potentially migrated from the interior to the surface. From Figure 2 (a), the granular surface morphology with uniform small grains were observed in BFO_O film. Obvious voids were located at the grain boundaries, deteriorating the densification of the BFO_O film and its electric properties.

The X-ray photoelectron spectroscopy (XPS) spectrum of O1s core levels of BFO_O and BFO_N thin films are shown in Figure 3. A strong peak at ~529.5 eV was observed for BFO_O and BFO_N thin films, which corresponds to oxygen in the perovskite lattice (O_L). The peak at ~531.2 eV was the surface-absorbed oxygen (O_A) [23]. To verify this, the surface of BFO_O and BFO_N films were etched with a thickness of ~ 3nm. No peaks can be obtained at ~531.2 eV in the interior BFO_O and BFO_N thin films. Furhemore, no obvious oxygen vacancies peak was observed in BFO films, which maybe related to the low amount of oxygen vacancies in BFO films annealing in a rapid thermal annealing furnace in air.

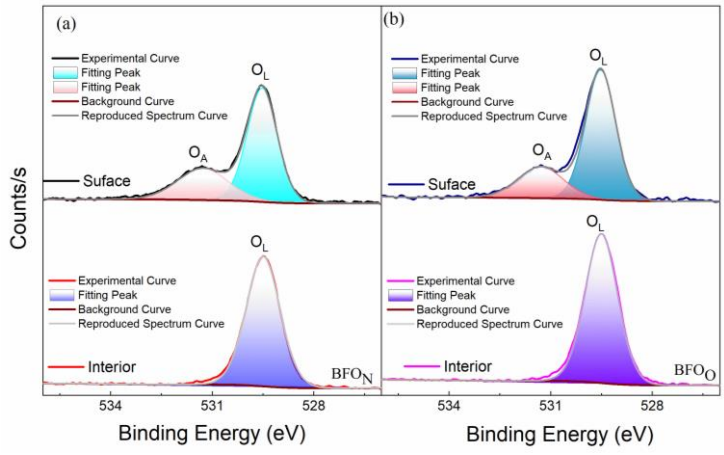

 doi:10.20944/preprints202408.0798.v1

Figure 3. (a) and (b) are the the XPS spectra of O 1s core level for the surface as well as interior BFO_O and BFO_N thin films, respectively.

3.1.2. Room Temperature Electrical Properties

Figure 4 shows the electrical properties of BFO_O and BFO_N films at 440 ± 5°C. Figure 4(a) and (b) presents the typical P-E loops of the $BiFeO_3$ films. When the applied electric field was sufficiently large, well rectangular-shaped, saturated P-E hysteresis loops were observed in the BFO_N and BFO_O film. A large remanent polarization (P_r~78.1 μC/cm²) and high rectangularity (~91.3%) of the hysteresis loop was observed in the BFO_N film at the applied electric field of 1165.2 kV/cm. A high remanent polarization (P_r~79.6 μC/cm²) and decent rectangularity (~86.8%) of the hysteresis loop was observed in the BFO_O film at the applied electric field of 915.4 kV/cm. Compared to the BFO_N film, the P-E loops of the BFO_O film displayed a somewhat roundish shape, indicating contributions from the leakage current induced by the voids and more grain boundaries [25]. The normalized pulsed polarization （ΔP=P* (switched polarization)-P^ (nonswitched polarization） with retention time and switching cycles were shown in Figure 4 (c) and (d). Both the BFO_N and BFO_O films exhibited good charge-retaining ability for up to 1.0 × 10^3 s. The improved charge-retaining ability (~1% loss) in the BFO_N film compared to that (~4% loss) for the BFO_O film was attributed to the reduced domain backswitching induced by the grain boundary defects and voids in the former than the latter [25]. As shown in Figure 4(d), good fatigue resistance up to 1.0 × 10^9 switching cycles was observed in both the BFO_N and BFO_O films, which could be attributed to the improved interface by using Al substrates as well as the low oxygen vacancies as discussed in Figure 3.

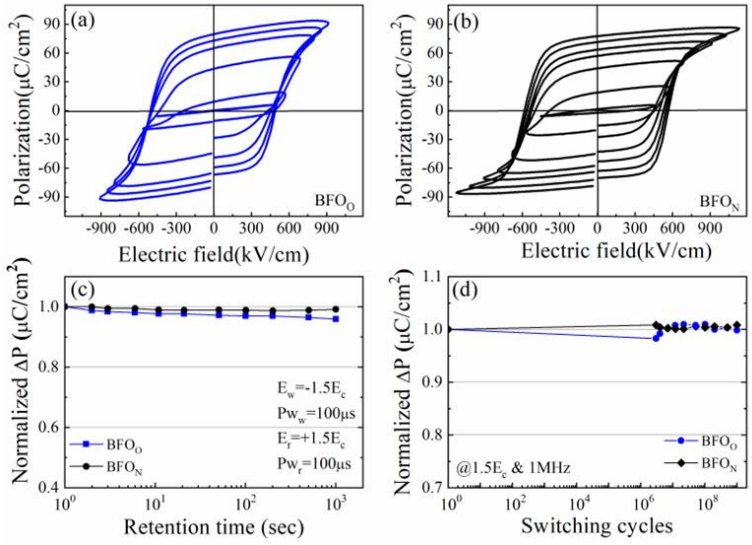

Figure 4. (Color online) Room-temperature polarization-electric field (*P-E*) curves for **(a)** the *BFO_O* and **(b)** *BFO_N* films at 440 ± 5°C; **(c)** retention and **(d)** fatigue properties investigated for the *BFO_O* and *BFO_N* films at 440 ± 5°C.

The leakage performances for BFO_O and BFO_N films are shown in Figure 5, the soaking time was 500 ms during leakage test under the unswitched linear mode [26]. From Figure 5 (a) and (b), we can see that the leakage current density (J) of BFO_N film was slightly higher than 1 time that of BFO_O film but less than 2 times, which can be ascribed to the slightly lower oxygen vacancy concentration in BFO_O film as discussed in Figure 3. To clarify the dominant leakage mechanism involved in BFO films, the linear fitting of leakage behaviors are shown in Figure 5(c)-(f) based on leakage mechanisms formulas [27]. From Figure 5(c) and (e), the Fowler-Nordheim tunneling (FN tunneling) [$\ln(J/E^2) \propto 1/E$] mechanism induced by the interface electrons activated into the conduction band by tunneling involved in BFO_N film under the positive electric field (<251.0 kV/cm) [28,29]. The FN tunneling mechanism observed at low electric field maybe related to the good crystallization of BFO_N film. The Ohmic conduction mechanism ($\log J \propto \log E$) can be observed at high electric field (>251.0 kV/cm),

 doi:10.20944/preprints202408.0798.v1

which should be related to the free oxygen vacancies in the film under the positive electric field. With increasing the electric field, the electrons transitioning from the interface to the body may form defect complexes with oxygen vacancies. The formation of defect complexes suppressed the electron transition from the interface to the conduction band and changing the leakage mechanism [30]. During the negative electric field, FN tunneling mechanism (<326.3 kV/cm) and space-charge-limited conduction (SCLC) (log J∝2log E) were involved in the leakage behavior of BFO_N film. From Figure 5(d) and (f), the SCLC mechanism (< 100.4 kV/cm) and the FN tunneling mechanism (>100.4 kV/cm) were predominant under positive electric field. The Ohmic conduction mechanism (<150.6 kV/cm) and FN tunneling mechanism (>150.6 kV/cm) can be observed under the negative electric field.

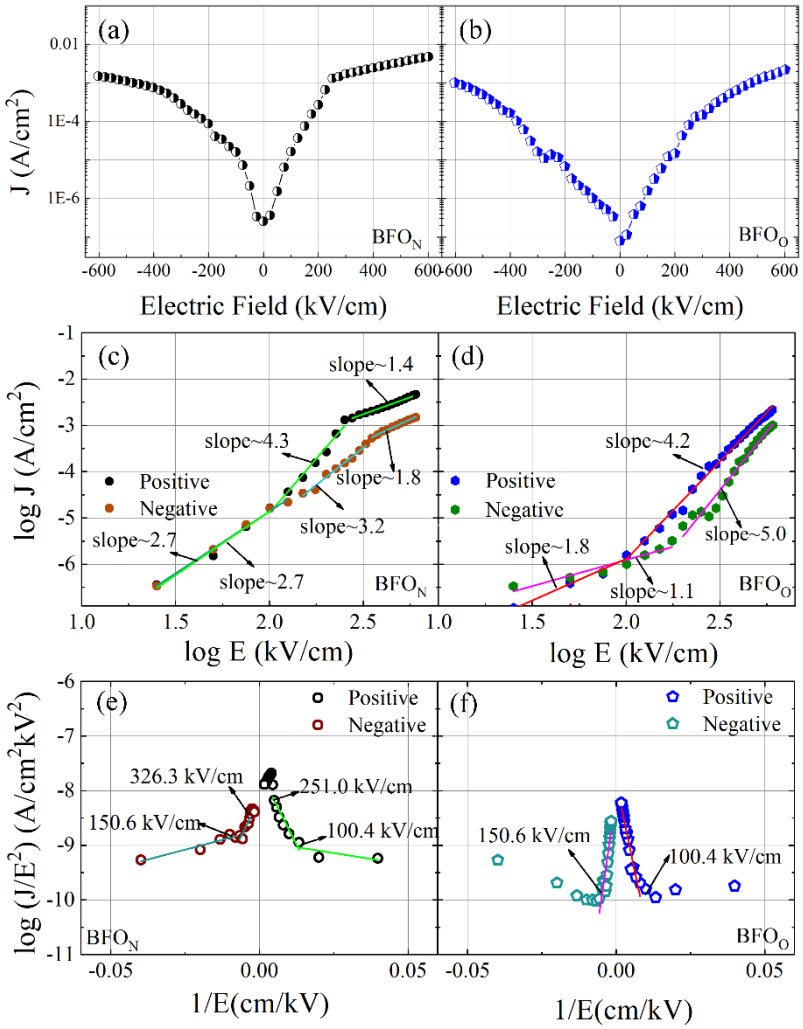

Figure 5. (Color online) **(a)** and **(b)** are the leakage current density-electric field (J-E) curves for BFO_O and BFO_N films annealed at 440 ± 5°C, respectively. **(c)** -**(f)** are curve fitting results of the J-E curves in Figure 5 (a) and (b).

According to the above discussion, it can be concluded that by adopting an N_2-rich atmosphere, improved crystalline quality could be achieved in the BFO films at 440 ± 5°C, resulting in better ferroelectric properties. Furthermore, a lower annealing temperature was expected for the $BiFeO_3$ films with Al substrates and an N_2-rich atmosphere. Therefore, an attempt was made to fabricate the BFO films below the annealing temperature of 400 °C. Finally, BFO films with decent electric properties were achieved a low temperature of 365 ±5°C (BFO_{N365}) on Al substrates under an N_2-rich atmosphere. The detailed properties of the BFO_{N365} film are shown in Figs. 6 and 7.

3.2. Performance of $BiFeO_3$ Film under an N_2-Rich Atmospheres Annealed at 365 ± 5 °C

3.2.1. Microstructure Analysis

 doi:10.20944/preprints202408.0798.v1

The XRD 2θ-scan pattern and surface SEM image of the BFO_{N365} film are shown in Figure 6. A bulk-like random polycrystalline structure with obvious (100), (110)/(104) peaks was observed, indicating that the BFO films were crystallized even at a low annealing temperature of 365 ±5°C. A dense morphology with fine nanograins were clearly revealed, indicating that the film has crystallized at this low annealing temperature.

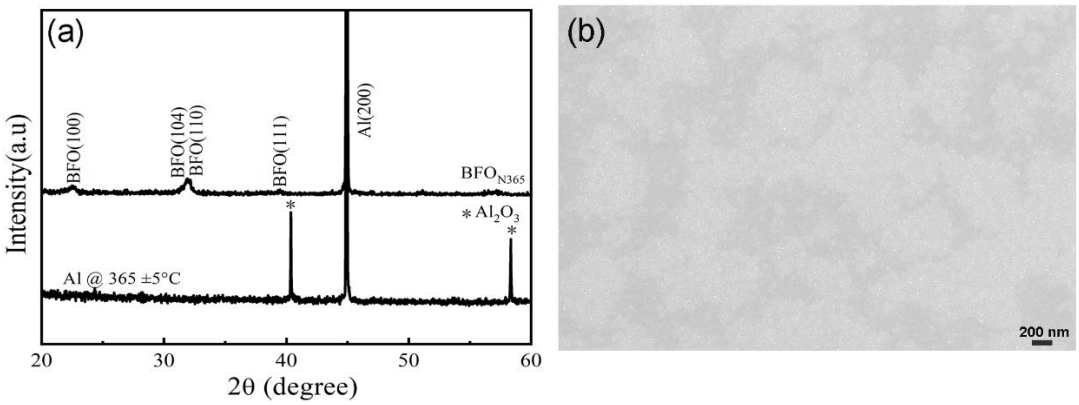

Figure 6. XRD 2θ-scan patterns (a) of the BFO_{N365} film and Al foil annealed at 365 ±5°C and surface SEM image (b) of the BFO_{N365} film.

3.2.2. Room Temperature Electrical Properties

Typical P-E loops were observed in Figure 7(a) for the BFO_{N365} film, and a sizable remnant polarization (P_r~70 μC/cm²) and decent rectangularity (~75.0%) of the hysteresis loop at the applied electric field of 1118.1 kV/cm were obtained. These observations indicated that Al foil served as a suitable substrate for fabricating ferroelectric $BiFeO_3$ films under low annealing temperatures. As shown in Figure 7(b), the leakage current density of BFO_{N365} was lower than ~1×10^{-4} A/cm² under the electric field of 353.5 kV/cm. Figure 6(c) and (d) illustrates that good fatigue resistance with a low loss (~5.8%) up to 1.0×10^9 switching cycles for positive polarization was observed, and the loss for negative polarization under the same testing conditions was ~27%. Retention testing was carried out for BFO_{N365} films, a degradation of ~29% for the negative polarization was observed after 1.0×10^3 s, which is much higher than that for the positive polarization (~14%). The improved fatigue and retention performance at the positive side could be ascribed to the reduced interfacial defects (e.g. vacancies, grain boundaries or amorphous regions) at the bottom electrode under a long exposure to a processing temperature. The achieved ferroelectric characteristics of the BFO film directly deposited on the substrate without a buffer layer under the temperature of 400 °C have not yet been reported. This was attributed to the N_2-rich atmosphere, the Al foil substrate, as well as the homogeneous precursor solution.

 doi:10.20944/preprints202408.0798.v1

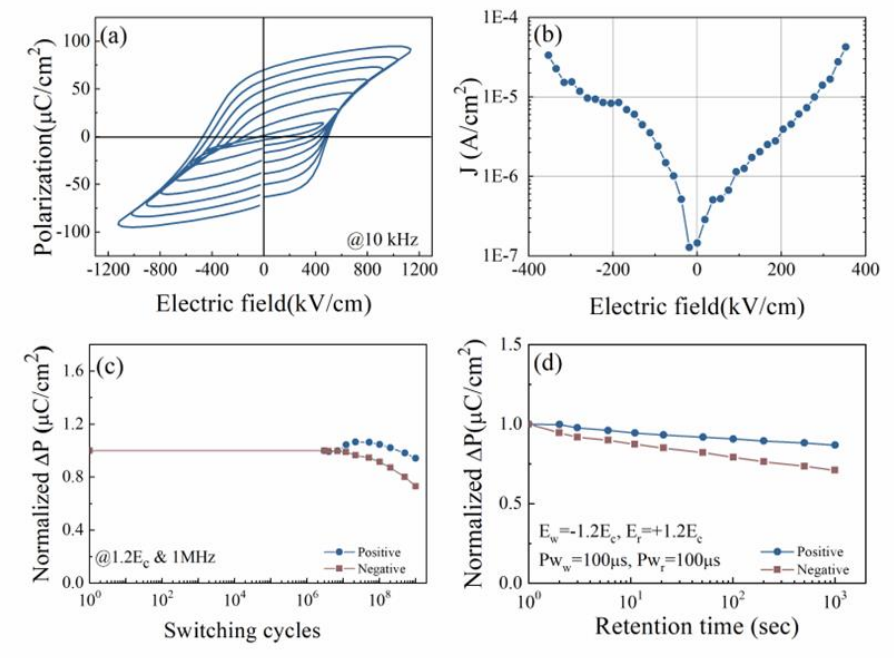

Figure 7. (Color online) Room-temperature **(a)** P–E curves, **(b)** leakage property, the normalized pulsed polarization as a function of **(c)** switching cycles and **(d)** the retention time for the BFO_{N365} film.

4. Conclusions

In summary, the BFO films were successfully fabricated at low annealing temperature (< 450 °C). A common base metal, aluminum foil was adopted as the bottom electrode and substrate for BFO ferroelectric film. Compared to an oxygen-rich atmosphere, a nitrogen-rich atmosphere was more conducive to optimizing the performance of BFO films. Along with excellent retention and fatigue properties, *P-E* loops with a large P_r value (~78.1 μC/cm²) and high rectangularity (~91.3%) at the applied electric field of 1165.2 kV/cm were obtained in the BFO films deposited under an N_2-rich atmosphere at 440 ± 5°C. By using an N_2-rich atmosphere as well as the Al substrates, BFO films with decent electric properties were achieved a very low temperature of 365 ±5°C. This offers a new strategy for lowering the annealing temperature of BFO films.

Funding: This research was funded by the Natural Science Foundation of Shandong Province, grant number ZR2022ME075.

Data Availability Statement: Data are available upon request to the corresponding author.

Conflicts of Interest: The authors declare no conflicts of interest. The funders had no role in the design of the study; in the collection, analyses, or interpretation of data; in the writing of the manuscript; or in the decision to publish the results.

References

1. Wu, J.; Wang J. Orientation dependence of ferroelectric behavior of $BiFeO_3$ thin films. *J. Appl. Phys.* **2009**,106, 104111. https://doi.org/10.1063/1.3261841.
2. Yan J.; Ouyang J.; Cheng H.B.; Yan P. Low temperature deposition of $BiFeO_3$ films on Ti foils for piezoelectric applications. *Scripta Materialia* **2021**, 204, 114152. https://doi.org/10.1016/j.scriptamat.2021.114152.
3. Wang, J.; Neaton, J. B.; Zheng, H.; Nagarajan, V.; Ogale, S.B.; Liu, B.; Viehland, D.; Vaithyanathan, V.; Schlom, D.G.; Waghmare, U.V.; Spaldin, N.A.; Rabe, K.M.; Wuttig, M.; Ramesh, R. Epitaxial $BiFeO_3$ multiferroic thin film heterostructures. *Science* **2003**, 299, 1719–1722. https://doi.org/10.1126/science.1080615.

4. Wu, J.G.; Fan, Z.; Xiao, D.Q.; Zhu, J.G.; Wang, J. Multiferroic bismuth ferrite-based materials for multifunctional applications: Ceramic bulks, thin films and nanostructures. *Prog. Mater. Sci.* **2016,** 84, 335–402. https://doi.org/10.1016/j. pmatsci.2016.09.001.
5. Yang, B.B.; Jin, L.H.; Wei, R.H.; Tang, X.W.; Hu, L.; Tong, P.; Yang, J.; Song, W.H.; Dai, J. M.; Zhu, X.B.; Sun, Y.P.; Zhang, S.J.; Wang, X.L.; Cheng, Z.X. Chemical solution route for high-quality multiferroic $BiFeO_3$ thin films. *Small* **2021,** 17,1903663. https://doi.org/10.1002/smll.201903663.
6. Catalan, G.; Scott, J.F. Physics and applications of bismuth ferrite. *Adv. Mater.* **2010,** 21, 2463–2485. https://doi.org/10.1002/adma.200802849.
7. Zhu, H.F.; Yang, Y.L.; Ren, W.; Niu, M.M.; Hu, W.; Ma, H.F.; Ouyang, J. Rhombohedral $BiFeO_3$ thick films integrated on Si with a giant electric polarization and prominent piezoelectricity, *Acta Materialia* **2020,** 200, 305–314. https://doi.org/10.1016/j.actamat.2020.09.022.
8. Tomczyk M; Bretos I.; Jiménez R.; et al. Direct fabrication of $BiFeO_3$ thin films on polyimide substrates for flexible electronics. *Journal of Materials Chemistry C,* **2017**, 5(47), 12529-12537. https://doi.org/10.1039/C7TC04571A.
9. Wen, Z.; Shen, X.; Wu, J.X; Wu, D.; Li, A.D.; Yang, B.; Wang, Z.; Chen, H.Z.; Wang, J.L. Temperature-dependent leakage current characteristics of Pr and Mn cosubstituted $BiFeO_3$ thin films, *Appl. Phys. Lett.* **2010,** 96,202904. https://doi.org/10.1063/1.3432083.
10. Yan, J.; Hu, G. D.; Chen, X. M.; Wu, W. B.; Yang, C. H. Ferroelectric properties, morphologies, and leakage currents of $Bi_{0.97}La_{0.03}FeO_3$ thin films deposited on indium tin oxide/glass substrates, *Journal of applied physics* **2008,** 104, 076103. https://doi.org/10.1063/1.2975321.
11. Chen, D.Y.; Chen, Z.H.; He, Q.; Clarkson, J.D.; Serrao, C. R.; Yadav, A. K.; Nowakowski, M.E.; Fan, Z.; You, L.; Gao, X.S.; Zeng, D.C.; Chen, L.; Borisevich, A.Y.; Salahuddin, S.; Liu, J.M.; Bokor, J. Interface engineering of domain structures in $BiFeO_3$ thin films, *Nano Letter* **2017**,17, 486–493, https://doi.org/10.1021/acs.nanolett.6b04512.
12. Jang, H. W. ; Ortiz, D. ; Baek, S. H. ; Folkman, C. M. ; Das, R. R. ; Shafer, P. ; Chen, Y.B. ; Nelson, C. T. ; Pan, X.Q. ; Ramesh, R. ; Eom, C.B. Domain engineering for enhanced ferroelectric properties of epitaxial (001) BiFeO thin films. *Advanced Materials* **2009**, 21, 817-823. https://doi.org/ 10.1002/adma.200800823
13. Yan, J.; Zhu, H. F.; Ouyang, J.; Kanno, I.; Yan, P.; Wang, Y.Y.; Onishi, K.; Nishikado, T. Highly (00l)-textured $BiFeO_3$ thick films integrated on stainless steel foils with an optimized piezoelectric performance. *Journal of the European Ceramic Society* **2022**, 42, 3454-3462. https://doi.org/10.1016/j.jeurceramsoc.2022.03.011.
14. Chen, X.M.; Hu, G.D.; Wang, J.C.; Cheng, L.; Yang, C.H.; Wu, W.B. Thickness effects of $Bi_{0.89}Ti_{0.11}FeO_3$ thin films deposited on $PbZr_{0.2}Ti_{0.79}Nb_{0.01}O_3$ buffer layers. *J. Alloy. Compd.* **2011,** 509, 431-434. https://doi.org/10.1016/j.jallcom.2010.09.049.
15. Li, H.; Ding, Y.W.; Ren, K. J.; Zeng, Z.X.; Chen, C.; Deng, X.L.; Gao, R.L.; Cai, W.; Wang, Z.H.; Fu, C.L.; Lei, X.; Chen, G.; Effect of rapid/slow annealing routes on the magnetic and photoelectric properties of $BiFeO_3/CoFe_2O_4$ multilayer thin films. *Journal of Alloys and Compounds* **2024**, 989, 174203. https://doi.org/10.1016/j.jallcom.2024.174203.
16. Pan, T.M.; Chen, Z. Y.; Weng, W. C.; Her, J.L.; Electrical and structural properties of $BiFeO_3$ thin films with four distinct buffer layers: La_2O_3, Pr_2O_3, Sm_2O_3, and Tm_2O_3. *Physica B: Condensed Matter*, **2024**, 689, 416219. https://doi.org/10.1016/j.physb.2024.416219.
17. Zhang, J.; Dai, J.Q.; Zhang, G.C.; Zhu, X. J.; Significantly improved ferroelectric properties of (Zn,Co) co-doped $BiFeO_3$ thin films prepared by sol-gel method. *Ceramics International* **2024,** 50, 28449-28457. https://doi.org/10.1016/j.ceramint.2024.05.151.
18. Wang, Y. P.; Zhou, L.; Zhang, M. F.; Chen, X. Y.; Liu, J. M.; Liu, Z. G. Room-Temperature Saturated Ferroelectric Polarization in $BiFeO_3$ Ceramics Synthesized by Rapid Liquid Phase Sintering. *Appl. Phys. Lett.* **2004,** 84, 1731–1733. https://doi.org/10.1063/1.1667612.
19. Palkar, V. R.; Pinto, R. $BiFeO_3$ thin films: novel effects. *Pramana J.Phys.* **2002,** 58, 1003–1008. https://doi.org/10.1007/s12043-002-0207-0.
20. Kingon, A.I.; Srinivasan, S. Lead zirconate titanate thin films directly on copper electrodes for ferroelectric, dielectric and piezoelectric applications. *Nat. Mater.* **2005,** 4, 233–237. https://doi.org/10.1038/nmat1334.
21. Hidnert, Peter; Krider, H. S. Thermal Expansion of Aluminum and Some Aluminum Alloys. *Journal of Research of the National Bureau of Standards* **1952,** 48, 209-220. https://doi.org/10.6028/jres.048.030.

22. Yim, W. M.; Paff, R. J. Thermal expansion of AlN, sapphire, and silicon. *J. Appl. Phys.* **1974,** 45, 1456–1457. https://doi.org/10.1063/1.1663432.
23. Niu, M.M.; Zhu, H.F.; Wang, Y.Y.; Yan, J.; Chen, N.; Yan, P.; Ouyang, J. Integration-friendly, chemically stoichiometric $BiFeO_3$ films with a piezoelectric performance challenging that of PZT. *ACS Appl. Mater. Interfaces* **2020,** 12, 33899–33907. https://doi.org/10.1021/acsami.0c07155.
24. Liu, H.Y.; Pu, Y.P.; Shi, X.; Yuan, Q.B. Dielectric and ferroelectric properties of $BiFeO_3$ ceramics sintered in different atmospheres. *Ceramics International* **2013,** 39, S217-S220. http://dx.doi.org/10.1016/j.ceramint.2012.10.065.
25. Lee, J. S.; Joo, S. K. Analysis of grain-boundary effects on the electrical properties of $Pb(Zr,Ti)O_3$ thin films. *Applied Physics Letters* **2002,** 81, 2602-2604. https://doi.org/10.1063/1.1511280.
26. Yan, J.; Jiang, X. M.; Hu, G. D. Leakage mechanisms of partially self-polarized $BiFeO_3$ film. *Ceramics International* **2018,** 44, 13765-13772. https://doi.org/10.1016/j.ceramint.2018.04.219.
27. Sun, W.; Zhou, Z.; Luo, J.; Wang, K.; Li, J. F. Leakage current characteristics and Sm/Ti doping effect in $BiFeO_3$ thin films on silicon wafers. *J. Appl. Phys.* **2017,** 121, 064101-7. https://doi.org/10.1063/1.4975784.
28. Luo, J. M.; Lin, S. P.; Zheng, Y.; Wang, B. Nonpolar resistive switching in Mn-doped $BiFeO_3$ thin films by chemical solution deposition. *Appl. Phys. Lett.* **2012,** 101, 062902-3. https://doi.org/10.1063/1.4742897.
29. Yang, H.; Wang, Y. Q.; Wang, H.; Jia, Q. X. Oxygen concentration and its effect on the leakage current in $BiFeO_3$ thin films. *Appl. Phys. Lett.* **2010,** 96, 012909-3. https://doi.org/10.1063/1.3291044.
30. Hu, G.D.; Fan, S.H.; Yang, C.H.; Wu, W.B. Low leakage current and enhanced ferroelectric properties of Ti and Zn codoped $BiFeO_3$ thin film. *Appl. Phys. Lett.* **2008,** 92, 192905-3. https://doi.org/ 10.1063/1.2918130.